Journal of Physiology - Paris 105 (2011) 71–82

Contents lists available at SciVerse ScienceDirect

Journal of Physiology - Paris

journal homepage: www.elsevier.com/locate/jphysparis

A modeling based study on the origin and nature of evoked post-synaptic local field potentials in granular layer

Harilal Parasuram [a], Bipin Nair [a], Giovanni Naldi [b], Egidio D'Angelo [c], Shyam Diwakar [a,*]

[a] Amrita School of Biotechnology, Amrita Vishwa Vidyapeetham (Amrita University), Amritapuri, Clappana P.O., 690 525, Kollam, Kerala, India
[b] Department of Mathematics, University of Milan, via Saldini 50, 27100 Milan (MI), Italy
[c] Department of Physiology, University of Pavia, via Forlanini 7, 21000 Pavia (PV), Italy

ARTICLE INFO

Keywords:
Evoked local field potential
Mathematical modeling
Granular layer
Cerebellum
LTP
LTD
Computational neuroscience

ABSTRACT

Understanding population activities of underlying neurons reveal emergent behavior as patterns of information flow in neural circuits. Evoked local field potentials (LFPs) arise from complex interactions of spatial distribution of current sources, time dynamics, and spatial distribution of dipoles apart underlying conductive properties of the extracellular medium. We reconstructed LFP to test and parameterize the molecular mechanisms of cellular function with network properties. The sensitivity of LFP to local excitatory and inhibitory connections was tested using two novel techniques. In the first, we used a single granule neuron as a model kernel for reconstructing population activity. The second technique consisted using a detailed network model. LTP and LTD regulating the spatiotemporal pattern of granular layer responses to mossy fiber inputs was studied. The effect of changes in synaptic release probability and modulation in intrinsic excitability of granule cell on LFP was studied. The study revealed cellular function and plasticity were represented in LFP wave revealing the activity of underlying neurons. Changes to single cell properties during LTP and LTD were reflected in the LFP wave suggesting the sparse recoding function of granule neurons as spatial pattern generators. Both modeling approaches generated LFP *in vitro* (Mapelli and D'Angelo, 2007) and *in vivo* (Roggeri et al., 2008) waveforms as reported in experiments and predict that the expression mechanisms revealed *in vitro* can explain the LFP changes associated with LTP and LTD *in vivo*.

1. Introduction

Populations of neurons generate extracellular currents due to electrical activity and an electrode usually reads the activity as a local field potential (LFP) signal. Progress in the interpretation of such signals is crucial for the understanding of neuronal mechanisms and activity. The activity in neuronal networks originates from the contribution of multiple interconnected neurons. Evoked local field potentials (LFP) are often recorded by electrophysiologists as a measurement of extracellular activity and in cerebellar granular layer as a population activity. Eccles (Brock et al., 1951) proposed that LFP and EEG activities are generated by summated postsynaptic potentials arising from the synchronized excitation of neurons. For the cerebellar granular layer, the current view is that EEG and LFPs are generated by synchronized synaptic currents, possibly through the formation of dipoles (Eccles, 1967). The local field potential (LFP) is composed of low-frequency extracellular voltage fluctuations that are thought to reflect synaptic potentials (Mitzdorf, 1985) and other slow electrical signals such as spike after-potentials and voltage-dependent membrane oscillations.

LFP has been used widely in recent years to link neural activity to perception and cognition, including sensory stimuli coding, perceptual binding, attention, and working memory. The local field potential is believed to represent the synchronized input into the observed area, as opposed to the spike data, which represents the output from the area (Mitzdorf, 1985; Haberly and Shepherd, 1973; Logothetis, 2002). The quick fluctuations are caused by short inward and outward currents due to action potentials. These quick changes are filtered out in LFP and only slow fluctuations are retained. The LFP is thus composed of the well sustained currents in the tissue, typical of the somato-dendritic components.

We have used a detailed network model to reconstruct the ensemble activity of the granular layer network. The main problems lay in reconnecting the subcellular and cellular properties of emerging collective responses *in vivo* onto the combinatorial nature of inputs, the presence of noise and the geometrical nature of the underlying circuitry. The validity of this approach was demonstrated in seminal works on LFP generation in the olfactory bulb (Bower and Woolston, 1983; Haberly and Shepherd, 1973; Rall and Shepherd, 1968). More recently, computational techniques were

* Corresponding author. Tel.: +91 476 2803116; fax: +91 476 2899722.
E-mail address: shyam@amrita.edu (S. Diwakar).

0928-4257/$ - see front matter © 2011 Elsevier Ltd. All rights reserved.
doi:10.1016/j.jphysparis.2011.07.011

applied to the hippocampus in the attempt at deciphering spike generation recorded in certain behavioral conditions (Gold et al., 2006, 2007; Bedard et al., 2004; Henze et al., 2000).

In this article, two main approaches to simulate and reconstruct evoked LFP were undertaken. One was to study whether we could use a single granule neuron as a model kernel for reconstructing population activity. Eccles (Eccles, 1967) proposed granule cells as source–sink dipoles during action potential generation due to flow of currents. In our first approach, therefore, the predominant nature of granule cells as dipoles was used to generate various extracellular currents and combining them, a population extracellular LFP was reconstructed. In the second approach, a model of granular layer network was used to extract local field potential from a single point close to the region of interest.

The main focus was to reconstruct granular layer evoked postsynaptic LFP waveform while studying the cellular mechanisms and their impact on the evoked LFP traces. The models could easily regenerate both *in vitro* and *in vivo* traces and the effects of inhibition on the network. The goal was to transfer the knowledge on known mechanisms in single cell and understand its impact on the network response. The work also studies linear superposition for estimating single neuron LFP from several contributing compartments or regions indicating its dependence on electrotonic properties of the measured regions of the neurons.

2. Methods

2.1. Calculation of extracellular potential

Previous methods (Gold et al., 2006, 2007; Bedard et al., 2004) indicate that neuropil was well modeled using an isotropic volume conductor with capacitive effect of the medium around (1–3000 Hz). From these previous studies and the nature of dense packing (Chan-Palay and Palay, 1972), we assume that cerebellar granular layer extracellular medium is mostly ohmic (Plonsey, 1969; Holt and Koch, 1999). The electric potential in the granular layer extracellular space is governed by Laplace equation:

$$\nabla^2 \emptyset = 0 \tag{1}$$

where Ø is extracellular potential, at boundary condition $(1/p)\emptyset = J_m \cdot J_m$ is the transmembrane current density and ρ is the extracellular resistivity. Modeling single granule neurons as point sources, I is single point source; the amplitude of I in an unbounded isotropic volume conductor is given by coulomb's law.

$$\emptyset = \frac{\rho I}{4\pi r} \tag{2}$$

Note 'r' is the distance from the source to the measurement point.

NEURON simulation environment (Hines and Carnevale, 1997) was used to compute extracellular potential of each compartment of granule cell model (Diwakar et al., 2009). NEURON solves node equation by applying Kirchhoff's current law (Hines and Carnevale, 2001). Intracellular potential at any point/location in the membrane is equal to the sum of transmembrane potential and the extracellular potential (see Eq. (3)). Standard extracellular mechanism (*Vext*) in NEURON adds two layers of RC compartments as extracellular mechanism to the compartmental model (see Fig. 1).

For a passive neuronal model, we assume for a compartment i, the potential at the outermost (RC) layer to innermost (RC) layer are given as $Vext[1]_i$, $Vext[0]_i$, and $V_i + Vext[0]_i$. Potential at the innermost node is denoted as $Vext[0]_i + V_i$.

Potential at intracellular node, 'i' with reference to two neighboring compartments $i-1$ and $i+1$ is given by

$$\frac{dV_i}{dt}C_m = V_{i-1} * \left(\frac{1}{Ra_i}\right) - V_i\left\{\left[\frac{1}{Ra_i}\right] + \left[\frac{1}{Ra_{i+1}}\right] + V_{i+1} * \left[\frac{1}{Ra_{i+1}}\right] - g_{pas} * [V_i - e_{pas}]\right\} \tag{3}$$

$$-\frac{dV_i}{dt}C_m + \frac{dVext[0]_i}{dt} * (C_m + xc) - \frac{dVext[1]_i}{dt} * xc = Vext_{i-1} * \left(\frac{1}{Ra_i}\right) - Vext_i * \left\{\left[\frac{1}{Ra_i}\right] + \left[\frac{1}{Ra_{i+1}}\right] + Vext_{i+1} * \left[\frac{1}{Ra_{i+1}}\right] + g_{pas} * [V_i - e_{pas}] - xg * (Vext[0]_i - Vext[1]_{i+1})\right\} \tag{4}$$

where V_i is the membrane potential (potential difference across the neuronal membrane), $Vext[0]_i$ is the extracellular potential of first layer/field, $Vext[1]_i$ is the extracellular potential of second layer/field. *Ra* is the axial resistance, *xc* is the extracellular capacitance, *xg* is the extracellular conductance and C_m is the membrane capacitance. Eq. (4) was derived by substituting *Vext* + *V* for the absolute potential and Eq. (5) was derived from rearranging Eq. (4).

$$-\frac{dVext_i}{dt}xc + \frac{dVext[1]_i}{dt} * (C_m + xc[1]) = Vext[1]_{i-1} * \left(\frac{1}{Ra[1]_i}\right) - Vext[1]_i * \left\{\left[\frac{1}{Ra[1]_i}\right] + \left[\frac{1}{Ra[1]_{i+1}}\right] + Vext[1]_{i+1} * \left[\frac{1}{Ra[1]_{i+1}}\right] + xg * Vext[0]_i - xg[1] * (Vext[1]_i - e\_extracellular)\right\} \tag{5}$$

Evoked local field potential of cerebellar granular layer was generated and tested with two approaches. In both methods, a detailed multi-compartmental granule cell model (Diwakar et al., 2009) was used to generate extracellular currents, which were then used to generate the evoked local field potential (LFP) (see Section 2.1).

Detailed multi-compartmental model of granule cell consisted of 52 active compartments including the soma with four dendrites and an axon (Diwakar et al., 2009) was used to generate all possible combinations of response patterns caused by synaptic activation through mossy fibers and Golgi cells. The currents generated by each compartment were then used to reconstruct the evoked local field potential through the extracellular mechanism implemented in NEURON (Hines and Carnevale, 1997) (see Section 2.2). This adds two additional electrical resistance–capacitance (RC) layers/fields to the cable model to measure the current that flows out of the cell (see Fig. 1).

Granule cell model was activated by MF synaptic activation patterns (Mapelli and D'Angelo, 2007; Roggeri et al., 2008). Estimated extracellular potential was in the range of −0.0123 to −0.781 μV, it reaches maximum at hillock and initial compartment of axon. We used individual extracellular potentials (which represent individual cells contribution to population behavior) to compute evoked local field potential. Population response based on the multiple granule cells was analyzed further using MATLAB (Mathworks, USA).

2.2. Evoked LFP reconstruction

The central goal of this study was to assess the utility of the evoked LFP signal reconstruction for evaluating the granular layer processing of neural information. In experiments, (see Mapelli and D'Angelo, 2007; Roggeri et al., 2008) the signal received from each granule cell by the tungsten electrode depends on the distance of the cell from the electrode. We used two main techniques to reconstruct evoked LFP. Since the nature of reconstruction of the evoked LFP was determined by the characteristic nature of underlying cells (see Fig. 2) the technique itself helped decode the activity of the

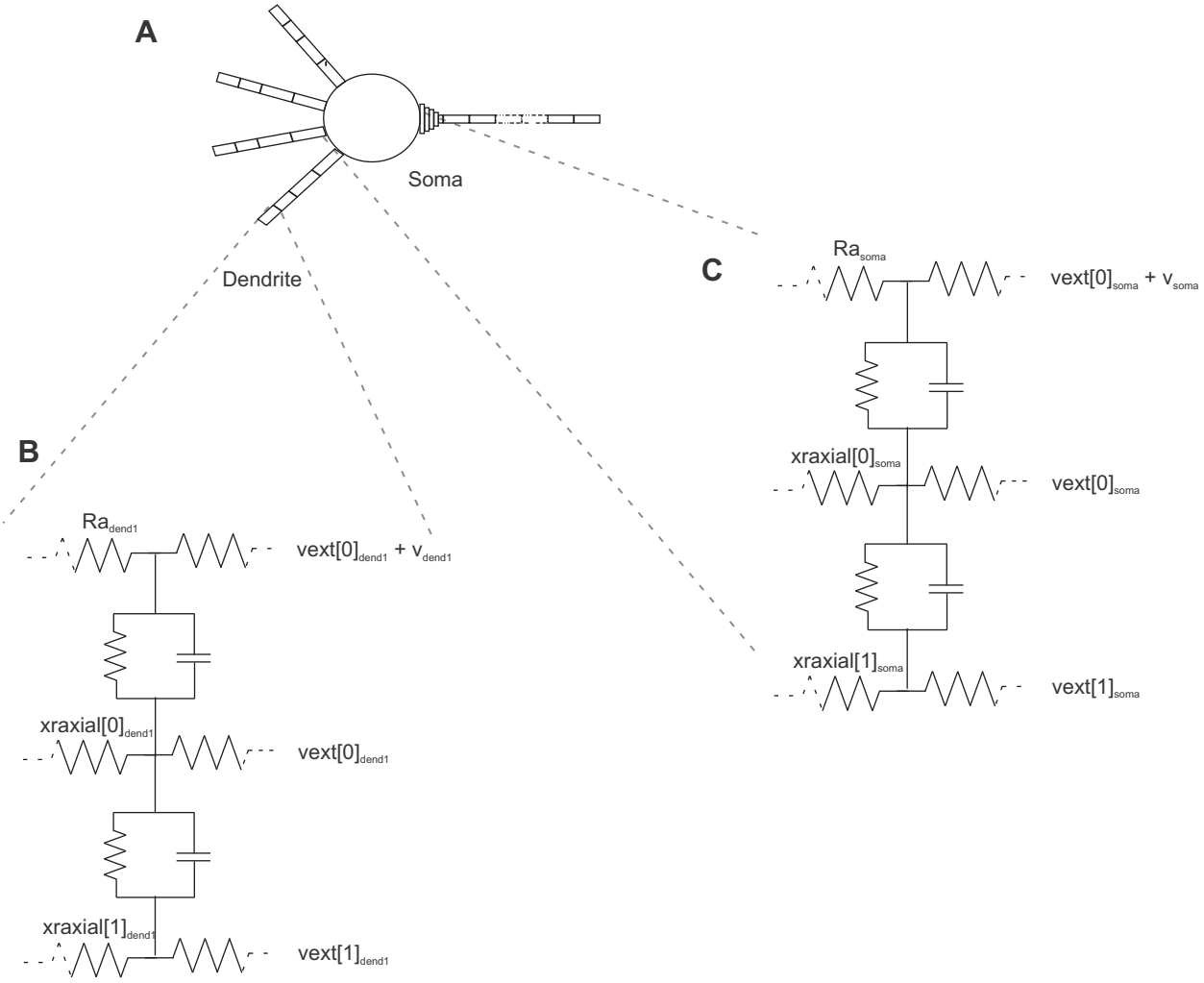

Fig. 1. Electrical equivalent circuit of granule cell model with extracellular mechanism (with two layers). (A) Schematic representation of granule cell model (Diwakar et al., 2009). Successive abstraction of extracellular circuit. Each compartment includes 2 R-C compartments representing the extracellular field in that compartment. Representative RC electric circuit shows the lumped electrical parameters of neuronal membrane corresponding to extracellular field in dendrite (B) and soma (C).

granular layer network. In both techniques (see Fig. 3A and B), the number of cells that contributed to the evoked LFP was estimated from previous works as 700 (*in vitro*, see Mapelli and D'Angelo, 2007) and 220 (*in vivo*, see Roggeri et al., 2008) respectively. The pattern ratios for generating the evoked response were based on a blind source separation analysis (Diwakar et al., 2011) on experimental traces. The distribution of granular layer cells in terms of mossy fiber excitation is shown in Table 1 (*in vitro*) and Table 2 (*in vivo*).

2.2.1. Technique 1 – Evoked LFP generation using single granule cell

The neural activity associated with the granule cell population inside the cerebellum has been investigated by recording action potentials of single and multiple units of the granule neuron model (Diwakar et al., 2009). Signal obtained was similar to the recorded potentials using a low impedance tungsten microelectrode *in vitro* (Mapelli and D'Angelo, 2007).

In this method, the electrotonic compactness of the granule cell (see D'Angelo et al., 1995, 1998, 2001) and the close packing of granular layer (Chan-Palay and Palay, 1972) was used to simplify the synchronous activity of the network. The population activity of the granular layer network was assumed to be sum of activities of the individual neurons. Since granule neurons are almost identical and synchronous (Vos et al., 1999), the possible outcomes were assumed to be combinations of various activation patterns that could affect individual neurons. A single neuron model was used to simulate various synaptic patterns and resulting output corresponded to a general evoked LFP postsynaptic wave as seen in granular layer. The outputs corresponding to various synaptic activation patterns were summed linearly with a noise term corresponding to the distance of the electrode from any particular cell. Some cells closer to the electrode were given none or less noise while cells further had lesser signal-to-noise ratio, due to temporal delay. The noise in the algorithm was implemented by padding zeros corresponding to time delay encoded by various errors. Computation of population evoked LFP is described in Section 2.3.

2.2.2. Technique 2 – Evoked LFP generation using granule cell population

Large scale *in vitro* network of granular layer in our model consisted of 700 detailed multi compartmental granule cells (Diwakar et al., 2009). Extracellular mechanism in NEURON (Hines and Carnevale, 1997) was inserted in all compartments to measure extracellular potentials. The sink–source effect (Eccles, 1967) hypothesized that the population of granule cells would generate typical field potential components based on action potential activity through the cell. Based on the underlying neuronal activity

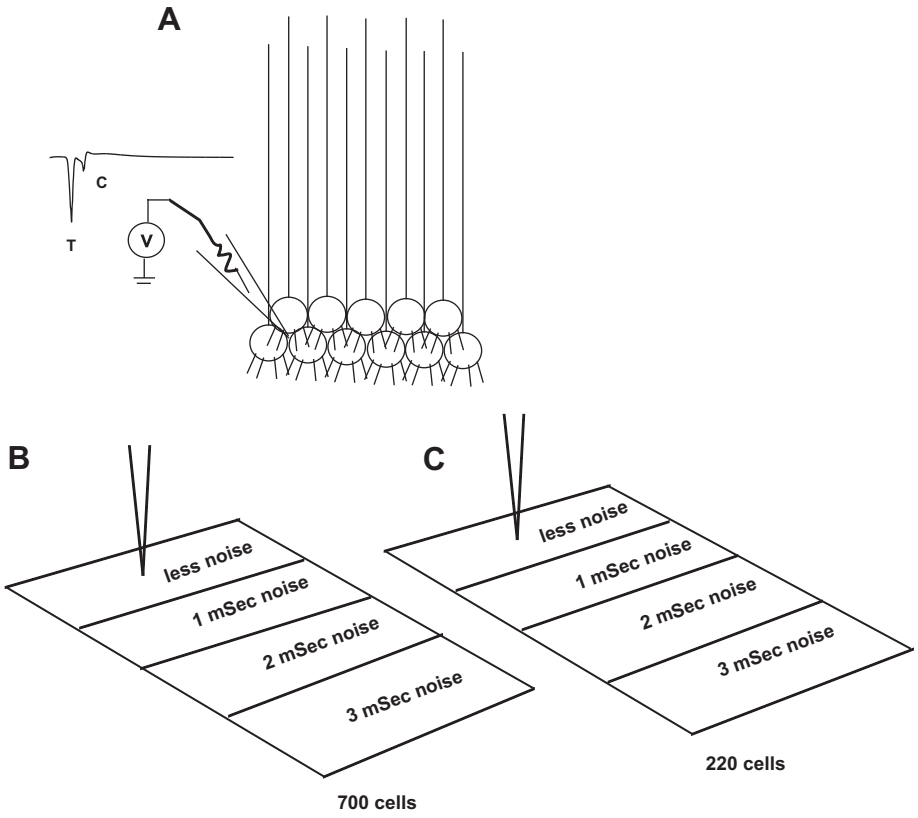

Fig. 2. Schematic diagram showing evoked LFP recording in granular layer. (A) The simulation includes modeling a measuring electrode close to the soma typically collects the extracellular components of somato-dendritic potentials of many cells (Roggeri et al., 2008). Distance-based noise for reconstructing evoked LFP (B and C). Assumptions in mathematical reconstruction show that via a recording electrode the evoked signal with varying combinations of mixtures with noise. A cell closer to measuring electrode sees more signal and lesser delay than extracellular potential from a cell further away. *In vitro* (single spikes through MF activating granule neuron clusters) measures evoked LFP (B) from approximately 700 cells and *in vivo* (burst through excitatory synapses) configuration measures evoked LFP (C) from approximately 220 cells.

(Diwakar et al., 2011) of the network, we categorized the cells to four main types of excitatory patterns (see Tables 1 and 2).

A smaller subset of the granular layer consisting of 220 cells (Diwakar et al., 2009) was used in the *in vivo* model of the network for evoked LFP reconstruction (see Fig. 2B and C). This estimate for cells was based on the glass electrode recordings of Roggeri et al. (2008).

The neurons were placed randomly and the measuring electrode was supposed to be the center. Any cell that was at a distance further away was assumed to contribute lesser to the generated LFP. Cells closer to the electrode had no or less noise and cells further had more noise or lesser signal-to-noise ratio. The implementation of temporal noise was same as technique 1.

2.3. Calculating evoked LFP

The modeling approach allows the activity of a number of neurons to contribute to the signal. The unfiltered signal reflects the sum of action potentials from cells in the recording region of interest (ROI). The low-pass filtering removed the excessive noise components from the signal. The model simulations were performed using NEURON (Hines and Carnevale, 1997) while LFP reconstruction was performed using Matlab (Mathworks, USA).

Eq6 denoted the process of shifting the recoded signal with respect to the noise, generated using pseudo random number generation algorithm implemented in Matlab (Mathworks, USA). Delays were assumed to be 0–3 ms with signal decay. The amount of noise was based on post-synaptic latency measurements (Silver et al., 1996) with a maximum of 3 ms delay. The electrode could measure cells that generated extracellular currents that came with a delay of 0–3 ms (see Fig. 2B). In the techniques, 1 ms was equated by padding 40 zeros ahead of the signal. Eq. (7) denoted the process of summing all shifted extracellular signals for all cells linearly.

$$\emptyset_{shifted,i}(t) = \emptyset_i(t - t') \tag{6}$$

$$\emptyset_{Evoked\,LFP}(t) = \sum_{i=0}^{n} \emptyset_{shifted,i}(t) \tag{7}$$

where $\emptyset_i\,(t)$ is the extracellular potential of ith cell in the neuronal population within the region of interest. $\emptyset_{shifted,i}\,(t)$ represents the extracellular potential shifted by time delay (0–3 ms) (see Silver et al., 1996). $\emptyset_{EvokedLFP}\,(t)$ was the final reconstructed signal by linearly summing the time-shifted extracellular potentials. n is the number of cells in the population based on the sensitivity of electrode (see Mapelli and D'Angelo, 2007; Roggeri et al., 2008). Here $n = 700$ for *in vitro* and $n = 220$ *in vivo* (see Fig. 2B and C).

Steps in computation:

Step 1: Set-up granular network with '*n*' neurons.
Step 2: Assign synaptic activation pattern to each cell corresponding to adequate percentage (see Table 1 for *in vitro* and Table 2 for *in vivo*).
Step 3: Randomly align the cells so measurement is a combination of all patterns.
Step 4: Extract $\emptyset_i\,(t)$, the extracellular potentials from somato-dendritic compartments as contribution of one cell.
Step 5: for each cell, compute

I. Random noise correlating to the distance from an electrode/measuring point of interest (delay, t').
II. Pad zeros before signal of that cell.

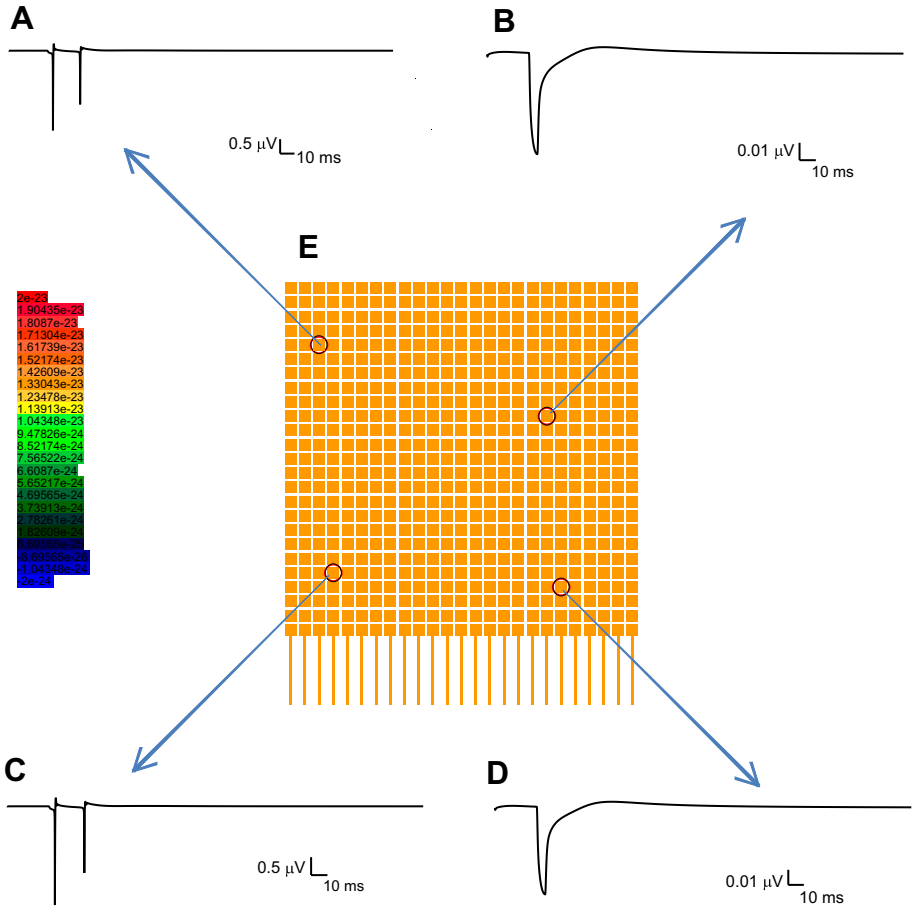

Fig. 3. Network contribution and *in vitro* LFP wave. Simulated evoked LFP for single spike inputs (*in vitro*) through MF. A–D are evoked LFP responses generated from single cells in the network. The full network model (E) with 700 cells. Based on data (Mapelli and D'Angelo, 2007; Diwakar et al., 2011), the ratio of excitatory cells are set to 5% with 1 MF, 45% with 2 MF, 35% with 3MF and 15% with 4MF synapses active. This ratio was set based on Blind source approximation techniques on data (Diwakar et al., 2011). A and C can be seen with both N_{2a} and N_{2b} waves while B and D shows N_{2a} alone. In some cases, such as in the presence of inhibition N_{2b} wave is suppressed.

Table 1
Types of synaptic combination of cells in *in vitro* network model.

Percentage of cells in the network	Number of excitatory synapse	Number of inhibitory synapse
15	1	1
35	2	2
35	3	3
15	4	4

Note 50% of the cells have 3 or 4 active excitatory synapses.

Table 2
Types of synaptic combination of cells in *in vivo* network model.

Percentage of cells in the network	Number of excitatory synapse	Number of inhibitory synapse
15	4	1
35	3	2
35	2	3
15	1	4

Note most cells have 2 or 3 active excitatory synapses. 4 predominant combinations were used.

Step 6: Sum all extracellular signals for all cells linearly with padded noise, $Ø_{EvokedLFP}$ (t). Total signal obtained is the reconstructed evoked LFP.

2.4. Simulation inputs and plasticity

Modeling evoked responses in brain slices *in vitro* was simulated by giving single spike as input via mossy fiber (MF) terminals. Evoked LFP in anaesthetized rat brain recordings *in vivo* was simulated as a burst of spikes via the MF input. Short burst implied five spikes per burst through MF and long burst implied nine spikes per burst. First spike latency was measured from the time of stimulus to peak of the spike. In *in vitro* simulations, the stimulus was applied at t = 20 ms. For *in vivo* simulations, a short burst corresponding to T wave was applied at t = 20 ms and a long burst for C wave at 60 ms.

To study effects of plasticity on the underlying population, we simulated plasticity in granule cells. Granule cell plasticity could be obtained by modifying intrinsic excitability and release probability (Holt and Koch, 1999; Nieus et al., 2006). In our models, we modified intrinsic excitability by changing ionic current density or gating. We modified the on–off gating characteristics of sodium channel to modify sodium activation and inactivation parameters (Diwakar et al., 2011) for higher and lower intrinsic excitability.

2.5. Post-processing

All simulations directly yielded the LFP waveform and simulations were performed on NEURON (Hines and Carnevale, 1997). The evoked LFP extracted from the model had a sampling rate of 40 kHz and was then filtered using Butterworth filter (Matlab,

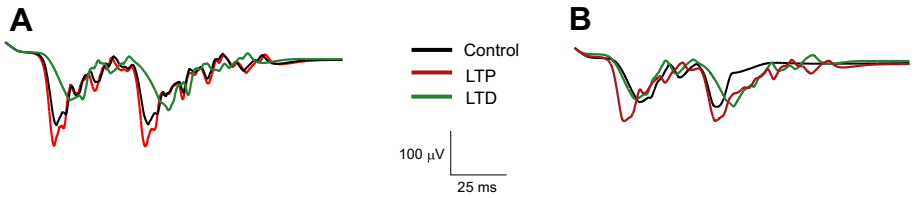

Fig. 4. Comparisons of reconstructing *in vivo* LTP-LTD. A shows the effects of LTP *in vivo* generated using single neuron approach. LTD (green), Control (black) and LTP (red) show small change in amplitude. Delay to peak (slope) also varies indicating the differential role of firing dynamics during plasticity and its reflection in evoked LFP. Evoked LFP *in vivo* (B) generated using network approach. The network consisted of 220 cells as in Roggeri et al. (2008). In this case, the ratio of excitation was set to with 15% with 1 MF, 35% with 2 MF, 35% with 3MF and 15% with 4MF synapses active (Mapelli and D'Angelo, 2007; Diwakar et al., 2011). LTP and LTD induction in A and B are through changes in intrinsic excitability and release probability (Holt and Koch, 1999). Each trace is the average of 15 simulations.

Mathworks, USA) with normalized cut-off frequency set at 4 kHz for *in vitro* LFP and 8 kHz for *in vivo*. Signal smoothing was performed using a Hilbert transform in Matlab (Mathworks, USA).

3. Results

Both algorithms could reconstruct evoked post-synaptic cerebellar granular layer *in vitro* LFP waveform indicated as N_{2a} and N_{2b} (Mapelli and D'Angelo, 2007) and *in vivo* waveform with T and C waves (Roggeri et al., 2008).

3.1. In vitro LFP reconstruction

Both algorithms successfully generated the field waveforms *in vitro* and *in vivo*, given their respective inputs. The *in vitro* components contained sharper information all of which the algorithms did not reproduce distinctly. In the model, the *in vitro* pattern was generated due to the spike based input via the mossy fiber (MF) synapses. At time = 20 ms, the MF synapses of the cells generate one spike to which the cell generates a post-synaptic response.

The post-synaptic response was varied as per input pattern and for a combination of 3MF and 4MF synaptic activation, spikes were observed. With 4MF synapses active, a doublet was seen (Diwakar et al., 2009) (see Fig. 3A and C). Correspondingly the responses generated N_{2a} wave and the doublet caused the N_{2b} wave. With inhibition at time = 24 ms via GABAergic synapses caused the suppression of the doublet and thereby suppresses the N_{2b} wave (Mapelli and D'Angelo, 2007).

Simulating with the *in vitro* inputs and with inhibition reduced, N_{2a} and N_{2b} peaks became more pronounced (see Fig. 3B).

3.2. In vivo LFP reconstruction

The *in vivo* evoked LFP response was reconstructed to produce the granular layer LFP generated by tactile stimulation (Roggeri et al., 2008). The evoked LFP was generated by bursts along mossy fiber terminals (Rancz et al., 2007; Chadderton et al., 2004; Jorntell and Eckerot, 2006). The *in vivo* evoked LFP signal consisted of two waves T (corresponding to trigeminal afferents), C (from cerebral cortex and pontine nuclei) produced by two bursts along the mossy fibers, one coming from the trigeminal pathway and other from the cortical pathway. T-wave in our models was generated by a short burst along the mossy fibers and C-wave by a longer burst that came much after the T wave (Roggeri et al., 2008). Our assumptions were that two separate clusters of granule cells generated the T and C waves (Roggeri et al., 2008). In our models, T-wave was generated by five spikes at 500 Hz along the MF synapses and C-wave by the nine spikes at 500 Hz via the MF synapses. Both methods (see Sections 2.2 and 2.3) reconstructed the *in vivo* LFP waveform (see Fig. 4, black trace).

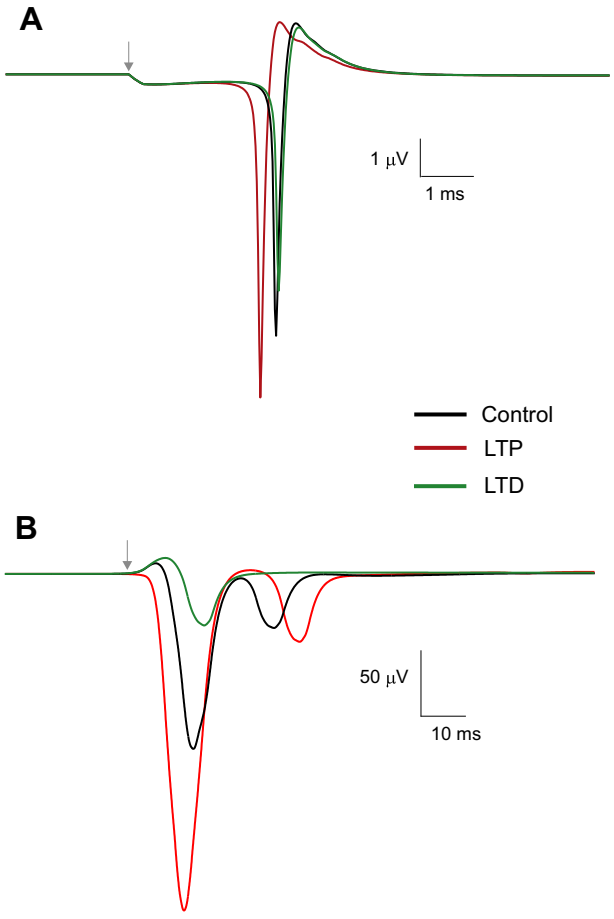

Fig. 5. Comparison of single cell and population responses. Evoked LFP was reconstructed and with the induction of different plasticity conditions. LTP (red trace) in single neuron (A) and population response (B) shows delay is far lesser and the extracellular potential is well pronounced. LTD (green trace) in single cells (A) affects the extracellular response less pronounced than seen in population (B). Control in both cases are shown (black trace).

3.3. Plasticity in LFP waveforms

Plasticity in LFP was experimentally shown in Roggeri et al. (2008). Given that release probability changes during long-term synaptic plasticity (D'Errico et al., 2010; Parasuram et al., 2010; Sola et al., 2004), simulating changes in intrinsic excitability of granule cells is equivalent to exploring the consequences of LTD or LTP.

With increased number of excitatory connections and higher intrinsic excitability, there was increased spike amplitude (as seen in LTP) and with low release probability and low intrinsic excitability (as in LTD), decreased spike amplitude was seen although the

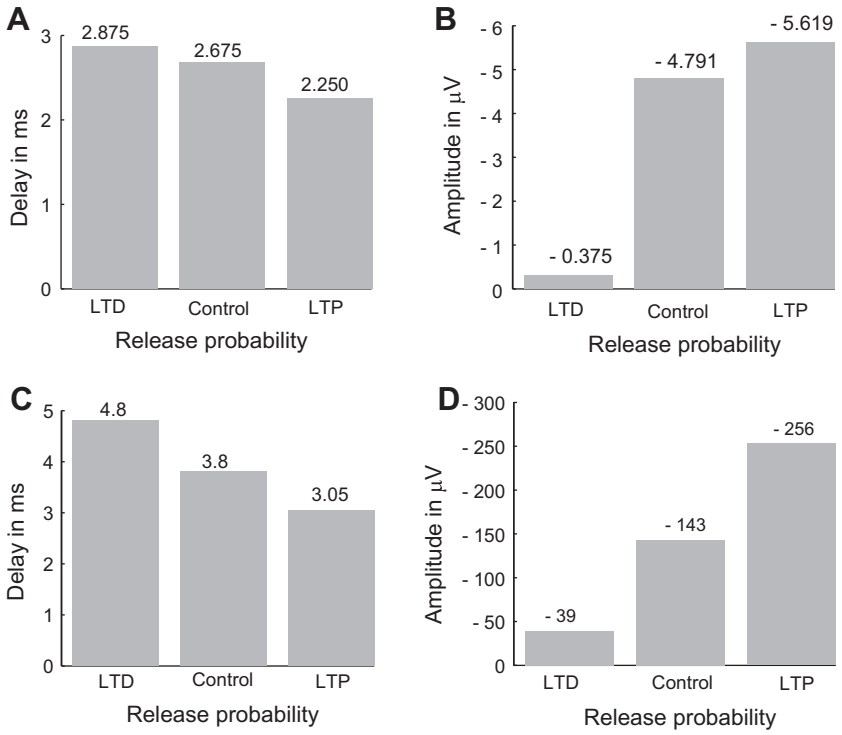

Fig. 6. Delay and latency in evoked response. Shows latency (A and C) and amplitude (B and D) comparison for different plasticity of single cell (A and B) and population (C and D). Note latency changes are more pronounced in population response (C) than in single neurons (A). The latency and amplitude changes suggest a coupled role of the intracellular mechanisms in the evoked response through modulation of firing dynamics.

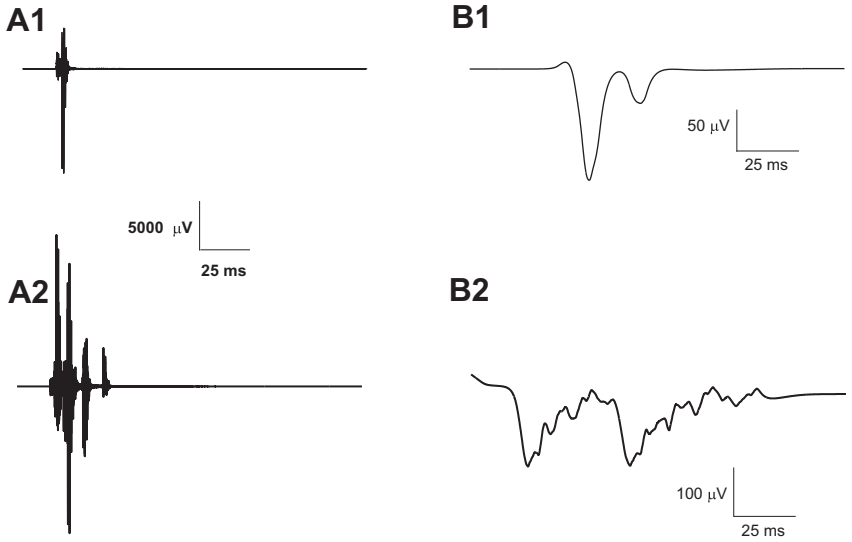

Fig. 7. Comparison of evoked LFP reconstruction using single compartmental and detailed models. *In vitro* (A1) and *in vivo* (A2) evoked LFP traces were generated using single-compartment granule neuron model (D'Angelo et al., 2001). *In vitro* (B1) and *in vivo* (B2) were traces generated using multi-compartment neuron model (Diwakar et al., 2009). A1 and A2 are unfiltered traces. Filtering removes most details and hence avoided in case of single compartment modeling scenario. B1, B2 were filtered at 4 and 8 kHz respectively. Although models could explain intracellular behavior (D'Angelo et al., 2001), electrotonic compactness was not sufficient to reproduce evoked LFP responses.

number of spikes is same (data not shown). Plasticity in granular layer is bidirectional (Jorntell and Eckerot, 2006). Since LFP comprised of spike information, the size and characteristics of reconstructed LFP was also changed.

Both algorithms showed the LFP changes *in vivo* although the single neuron approach (see Fig. 4A) distinctly showed the T, C wave components generated by the two independent bursts suggesting that the possibility of generation via two independent granule neuron populations.

The change in molecular mechanisms such as intrinsic excitability and release probability affected the amplitude of the T wave in terms of amplitude and delay (see Fig. 5).

With LTP, peak amplitude increased and delay decreased in the ensemble response vice versa was seen during LTD in comparison to the control (see Fig. 6). The changes in LTP was reflected similarly as with NMDA currents observed in single cell (Parasuram et al., 2010). Indeed coupling intracellular parameters such as AMPA and NMDA synaptic conductance with a detailed

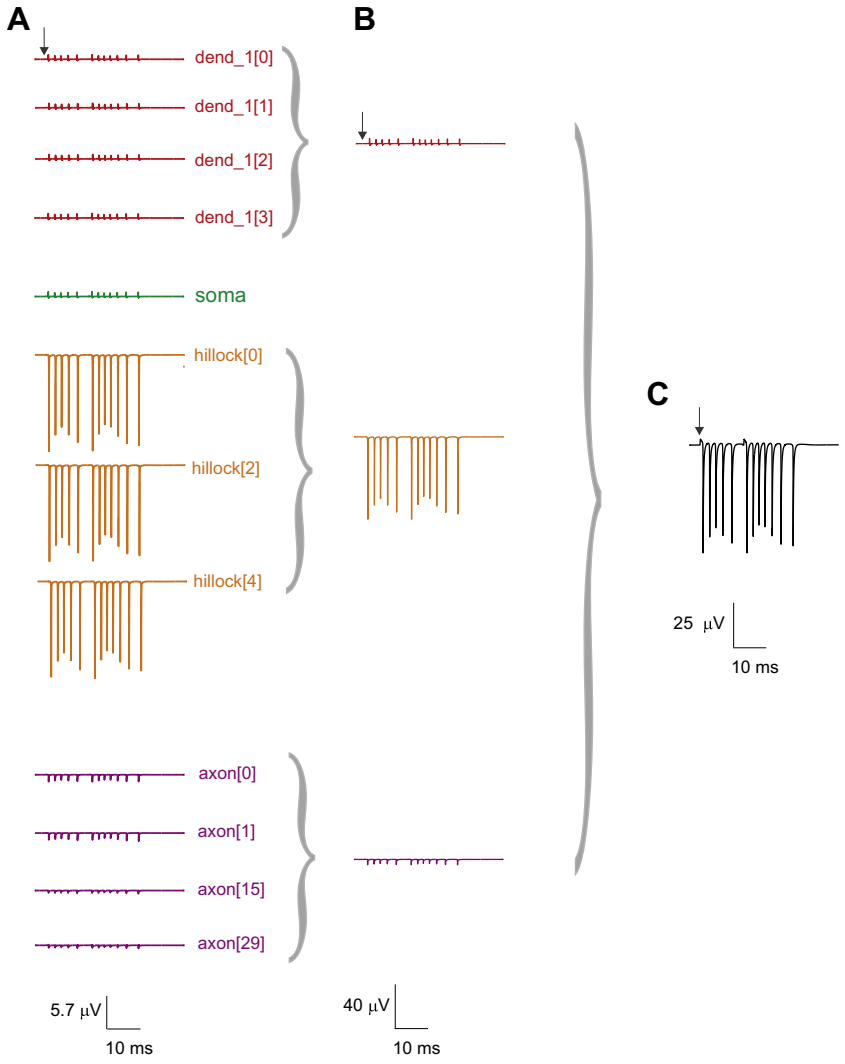

Fig. 8. Linear summation of extracellular components for single neuron evoked LFP response. Individual extracellular components (A) from different regions of the neuron contribute differently to single neuron evoked LFP. Here we sum the components directly to get the evoked response of a single neuron. Estimated single neuron evoked LFP for *in vivo* like burst inputs shows that extracellular behavior reflected intracellular firing dynamics. Stimuli input is indicated by the arrow. Note hillock compartments contribute maximum to LFP signal due to high density of Na^+.

reconstruction of granule cell intrinsic excitability (Diwakar et al., 2009; D'Angelo et al., 2001) reproduced the main aspects of granule cell synaptic excitation which in turn affected the evoked LFP response in terms of amplitude and delay. The model allowed dissecting the effect of presynaptic changes on firing and single granule electro responsiveness to evoked LFP response as in the neural ensemble. Like with single granule neurons, the theoretical prediction that either an increase in release probability or a change in g_{max} of the synaptic conductance could affect the evoked LFP response.

3.4. Impact of inhibition on LTP/LTD

The increase in active inhibitory connections to granule cells in the underlying network model decreased number of spikes, spike amplitude (especially during bursts when spike arises after the feedback inhibition from Golgi cell) and decreased spike latency. Decreasing GABAergic release probability (U_{inh}) from control value (0.34) showed an increase in number of spikes. Increase in the value of U_{inh} contributed to a reduction of the doublet to a single spike as seen *in vitro* (Mapelli and D'Angelo, 2007).

The evoked LFP *in vivo* wave reflected this change (see Fig. 6 of paper (Garwicz et al., 1998). With low inhibition, as predicted, the amplitude of T-wave increased and C-wave became more prominent. With increased inhibition the *in vitro* LFP wave became noisy and less defined (see Fig. 5B).

3.5. Unreliability of non-detailed models for LFP reconstruction

In granule neuron, electrotonic compactness was observed (D'Angelo et al., 1998) and electrical lumping amongst the soma-to-dendritic and hillock compartments has been observed (D'Angelo et al., 2001). Hence soma is main source of currents (D'Angelo et al., 1995, 1998) so a comparison was made for evoked LFP reconstruction using single compartment models (D'Angelo et al., 1995) in granular networks.

The results (see Fig. 7) indicated single compartmental models show inaccurate field potentials both in shape and amplitude. The *in vitro* case showed a single (negative) impulse instead of the N_{2a} which indicated that timing information alone may be retrieved from evoked LFP generated using single-compartmental models. Electrotonic compactness allowed models such as (D'Angelo et al., 2001) to clearly reproduce some of the intracellular

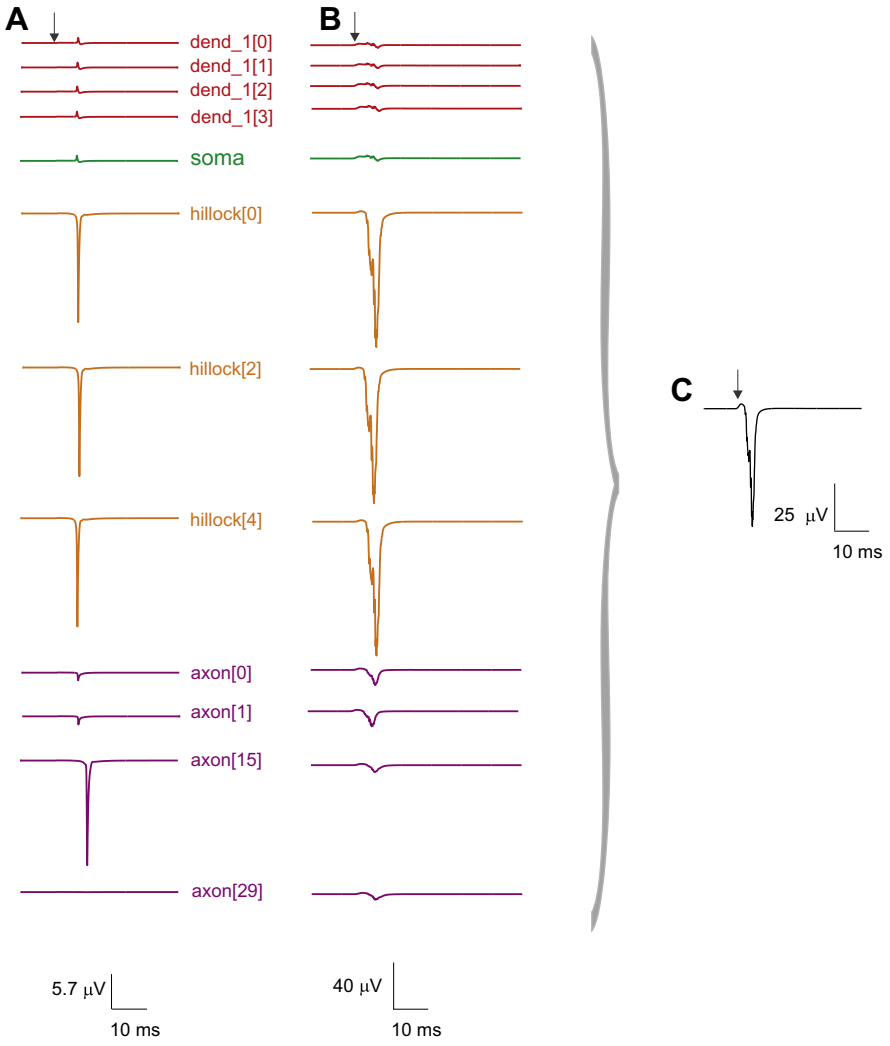

Fig. 9. Compartment-wise summation of extracellular components generating single neuron LFP. Note individual extracellular components from different regions of the neuron (A). Due to electrotonic behavior of the neuron, all dendritic components are summed together to estimate total dendritic contribution (B, top). Axonal and hillock regions are also summed independently (B) showing contributions due to localization of ion channels those compartments. Temporal delay in recording was estimated as noise and was added while summing the extracellular compartmental components. Estimated single neuron LFP (C) for *in vitro*-like spike inputs. Stimuli input are indicated by the arrow. LFP contributions from hillock remain same as in Fig. 5A (black trace).

properties. (Gold et al., 2007) has indicated constraining of models can be done through extracellular reconstructions. We found other techniques like LSA (Holt and Koch, 1999; Gold et al., 2006) may not correctly reproduce granular layer extracellular evoked LFP waves and their properties (data not shown).

3.6. Superposition dependency on electrotonic compactness of proximal regions

To understand if linear superposition would be realistic, we adopted two approaches to reconstruct LFP from compartmental components. In case 1, we summed the individual contributions of extracellular components of a single neuron (see Fig. 8) and then added the delay due to temporal noise to produce the evoked single neuron response.

In the second case, given each compartment has different density; we assumed that summing the neighboring compartmental components gave a better estimate of the evoked LFP (see Fig. 9). The electrotonic compactness of granule neurons (D'Angelo et al., 2001; Diwakar et al., 2009) indicated that some components can be lumped. Since many cells contribute to the evoked LFP each of the component's summed signal is perturbed by noise (like in Section 2.2.1, except at the compartment level). Temporal delays added smoothness to the signal probably due to ohmic filtering in the extracellular space (note Fig. 9C is better approximated than Fig. 8C at the single cell level).

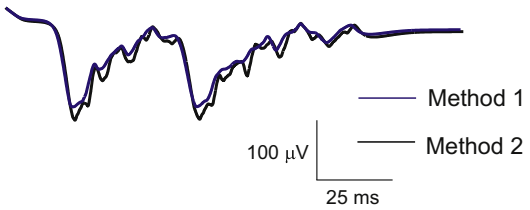

Fig. 10. Comparisons for linear superposition of extracellular components. (Blue) Population LFP generated by linear summation of extracellular components of many single neuron LFPs. (Black) Population LFP generated by linear summation of compartment-wise extracellular components from many proximal neurons. Note both LFPs look identical probably due to electrotonic compactness of somatodendritic compartments and electrical lumping with axonal initial segment.

Population LFP signal does not change much although latter case (generated using methods as in Fig. 8) seems more realistic

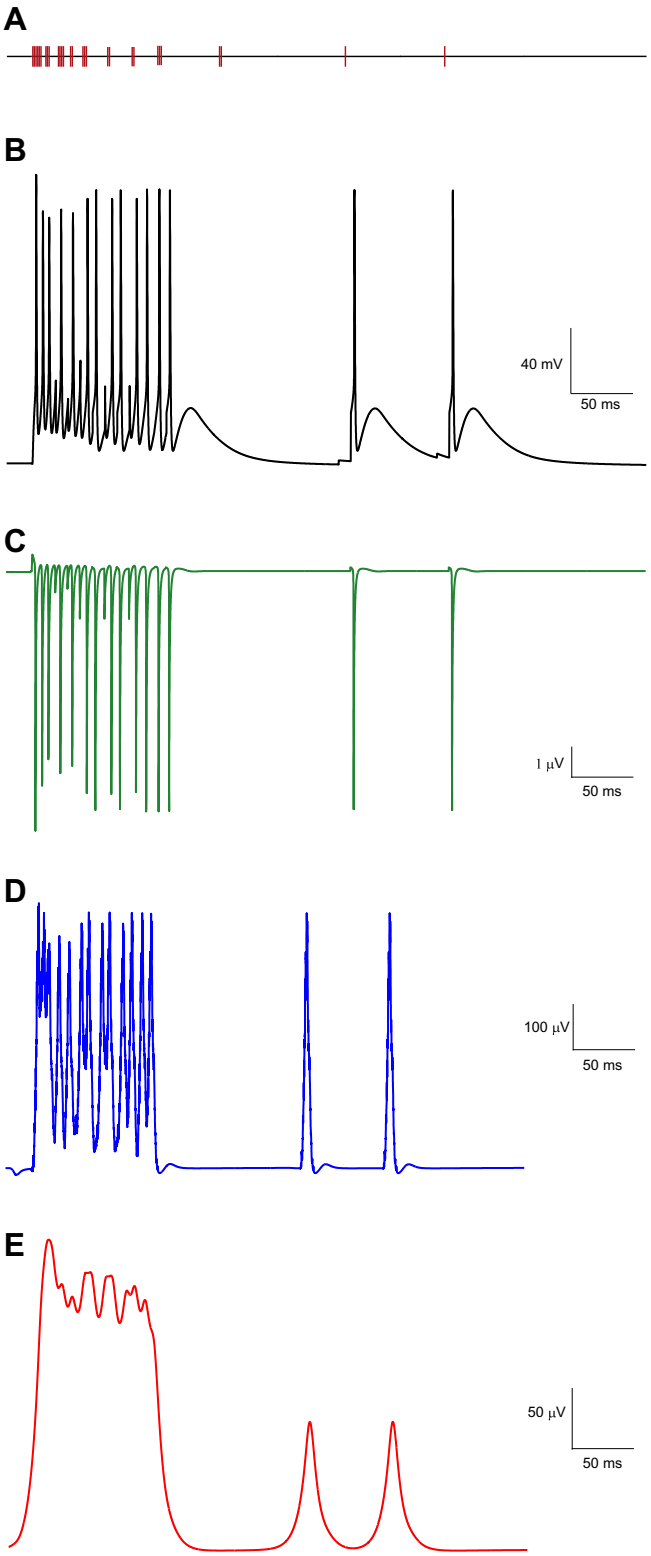

Fig. 11. Reconstruction of evoked response due to cutaneous stimulation. Cutaneous responses are predominantly evoked (Jorntell and Eckerot, 2006). (A) Input stimulus pattern given through mossy fiber (counted with respect to scale) corresponding to a manual cutaneous stimulation. Note the intracellular membrane voltage (B) of the cell response to the stimuli. Single granule neuron evoked LFP responses (C) closely correspond to the intracellular fluctuations in membrane potential (B). Inverted population evoked response (D) reconstructed from single cell approach (see Section 2.2.2). Filtered evoked population LFP at 5 kHz shows closeness to reported results (see Fig. 3D in Jorntell and Eckerot (2006)). Each trace is the average of 15 simulations.

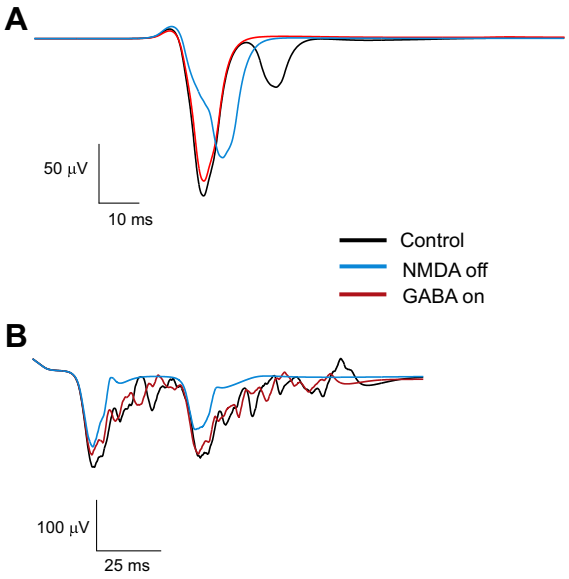

Fig. 12. Simulating pharmacological effects in evoked LFP wave forms. Changes in amplitude and width during control (black), Inhibition (red), NMDA off (blue) conditions *in vitro* (A). Note the N_{2b} is not observed in the presence of inhibition (red trace in A). Simulating the blocking of NMDA receptors reduced N_{2a} amplitude and cancelled N_{2b} (blue trace in A). Note the results are close to values reported in Mapelli and D'Angelo (2007). Changes in evoked LFP *in vivo* (B) during control (black). Since bursts–bursts transmission cause the T and C waves, the effect on inhibition (red trace) is not as prominent as A. Blocking NMDA receptors showed a sharp decrease in amplitude and increased latency on both T and C waves (blue trace, also see (Roggeri et al., 2008). Each trace is the average of 15 simulations. (For interpretation of the references to colour in this figure legend, the reader is referred to the web version of this article.)

suggesting evoked LFP can be generated through convolution schemes rather than linear summation. A comparison of the reconstruction of both techniques is shown in Fig. 10. Gold et al. (2006, 2007) studied the effects of constraining *in vivo* models with extracellular potentials. Size of the LFP wave suggested that each active compartment contributed differently in terms of amplitude of the field potential generated, verifying the hypothesis of Gold et al. (2006). The granule cell model (Diwakar et al., 2009) could be used directly without any extra constraints for extracellular LFP reconstruction.

The shape of the LFP near a single neuron depended on the closeness of the electrode. The nature of recorded evoked LFP response will depend on the closeness of the region proximal to measuring electrode. Thus an electrode close to axons will measure an inverted wave in comparison to an electrode close to soma or hillock.

The inaccuracy in reconstructing evoked LFP using superposition principle via linear summation may be overcome if the summation was substituted by convolution operation (such as with ReCONV algorithm (Diwakar et al., 2011).

3.7. Reconstructing in vivo cutaneous receptive fields

In order to understand the reproducibility of the methods and to test reconstruction of extracellular responses to cutaneous fields, we used our approach to generate the evoked LFP responses to *in vivo* cutaneous receptive field via spike activation. Cutaneous receptive fields are virtually absent of spontaneous activity (Garwicz et al., 1998). The reconstruction produced fields (see Fig. 11) similar to those previously reported in recordings. The mossy fiber pattern was adapted from raw steep histogram recordings (see Fig. 3C of Jorntell and Eckerot (2006)).

The simultaneous activation of mossy fibers (see Garwicz et al., 1998) generated reproduced the extracellular response (see Fig. 10).

The average amount of extracellular spikes in a single granule cell correlated with the behavior of the evoked response. Also simulating different types of synaptic activation patterns produced different evoked LFP patterns (data not shown), as reported in Jorntell and Eckerot (2006). Besides reproducibility, this observation supports the hypothesis that granule cells function as signal-to-noise-enhancing threshold elements with a specific type of input.

3.8. Predicting pharmacological effect on evoked LFP

The simulated field recordings showed the typical pharmacological changes observed experimentally (Roggeri et al., 2008).

In addition, the model predicted that the spike doublets in granule cells were the cause of N_{2a} and N_{2b} in the *in vitro* case (see Mapelli and D'Angelo, 2007). Without inhibition (Fig. 12A, black trace), N_{2b} wave was seen which is not seen when inhibition was present (Fig. 12A, red trace). Synaptic inhibition controlled the activation of the N_{2b} wave. NMDA was needed for the reconstruction of N_{2b} wave (Fig. 12A, blue trace).

In vivo simulations with T and C also showed unique behavior when inhibition was blocked (see Fig. 12B, red trace). A simulation without NMDA receptors (Fig. 12B, blue trace) strongly reduced the waves almost abolishing the ability of making spikes (D'Angelo et al., 1995). The pharmacological simulations suggest the correlation between cellular mechanisms *in vitro* (D'Angelo et al., 1995) and population code *in vivo*.

4. Discussion

Evoked post-synaptic local field potentials of the cerebellum granular layer have been effectively reconstructed employing two different approaches using the extracellular currents generated by a detailed multi-compartmental model of the granule cell (Diwakar et al., 2009). The effect of linear superposition of compartmental components in single neuron extracellular field has been illustrated. The main predictions *in vitro* include the role of inhibition in generating the N_{2b} wave, the modulatory effect of NMDA receptors and the reconstruction of changes due to plasticity in the evoked LFP through intracellular mechanisms. The other major prediction is the reconstruction of *in vivo* evoked response using mechanisms observed *in vitro* indicating the role of burst-burst transmission and feed-forward inhibition in granular layer.

The method shows that main errors of using single compartmental models (D'Angelo et al., 2001) for evoked LFP reconstruction, were related to the size of extracellular action potential, capacitive components and rapid changes in spiking. Signal degradation was seen while filtering LFP traces generated using single-compartment models. Relevant signal components were under-sampled thereby making the LFP generated from such models unreliable. Electrotonic compactness (D'Angelo et al., 1995; Diwakar et al., 2009) was not sufficient to reproduce granular layer evoked LFP response. This may cause problems when other methods such as LSA (Gold et al., 2006; Bedard et al., 2004) are used directly assuming granule cells as line sources.

Separate clusters of granule cells could independently generate *in vivo* waves and this was noted to reflect in both approaches. We assumed extracellular space in granular layer to be isopotential due to close packing of granule neurons. The simulations closely followed experimental results suggesting that there was not much non-linearity in the granular layer extracellular space. The nature of evoked LFP observed by variations in the nature of spike dynamics along with number of spiking cells could suggest that sparse coding could be preserved as suggested by Marr and Albus (Marr, 1969; Albus, 1971; Uusisaari and De Schutter, 2011).

The basic rules of granule cell plasticity (Holt and Koch, 1999; Nieus et al., 2006) were the changes of intrinsic excitability and release probability of synapses whose intracellular impacts were previously recorded. Plasticity in evoked LFP waves was nicely reproduced (Roggeri et al., 2008) by using the same mechanisms that were studied using intracellular techniques. Reconstructed evoked LFP observed after induction of LTP shows bigger amplitude and wider wave width while LTD shows the depression of width and lesser amplitude in the T–C components of the *in vivo* waveform. This observation suggests that LFP reflects the overall properties and mechanisms of spiking/non-spiking in single and in neuronal populations. Also, specific receptive fields may activate specific clusters of granule neurons (as seen in T and C waves) and may be regulated by the Golgi cell inhibition.

Linear superposition may not function if summation of individual local field potential compartments were used. As shown, ionic channel densities affected the evoked response components and hence proximity to the compartment with higher density defined the overall shape and nature of evoked LFP wave. This may however be overcome by novel techniques using convolution instead of linear summation at the multi-cell level. We would like to mention that the closeness or lack or differences amongst both cases could be due to the small size of neuron and its electrotonic compactness, suggesting linear summation of all compartment components of extracellular potentials may be misleading in case of bigger and geometrically-distributed neurons like Purkinje cell or the pyramidal cells. The methods used in reconstructing the simulations suggest the extracellular signal is a convolution of granular cell discharges and varied by the delay due to organizational connectivity (Diwakar et al., 2011).

However reconstructing extracellular properties indicate plasticity has similar mechanisms of regulation of granule cell burst initiation and thereby could implement an adaptable delay affecting downstream activation into circuitry. The role of single granule neurons in networks suggests that they play as signal-to-noise threshold elements (Bao et al., 2002) in the network in addition to the role in signal recoding.

Although other techniques have been successful in reconstructing extracellular potential, they often do not show what happens during plasticity or the role of single neurons in ensemble response. Our techniques allow reconstructing evoked LFP in small neurons. The main predictions are that like in individual granule neurons, the change in release probability and intrinsic excitability affected the evoked LFP response indicating that plasticity and feed-forward inhibition modulates the interplay of firing dynamics in neurons. Although additional plasticity roles may be played by other circuits that generate T and C waves, simulations suggest predominantly same mechanisms such as intrinsic excitability and release probability (Parasuram et al., 2010) may regulate the induction and nature of expressed plasticity.

5. Conclusion

The simulations indicate a large number of cells may be involved in coding the evoked LFP response (Roggeri et al., 2008). The role of inhibition and plasticity may help fine tune the "sparseness" of the code as indicated in Marr's theory (Uusisaari and De Schutter, 2011; Bao et al., 2002). To evaluate the exact role of firing, a closer view of cells in the region of interest may be needed. The experimental testing of these predictions will require further electrophysiological and imaging investigations of granular layer activity and computational modeling of the cerebellum (Solinas et al., 2010) and of the cerebro-cerebellar control loops (Uusisaari and De Schutter, 2011; Bao et al., 2002; Katz and Steinmetz, 1997).

Acknowledgments

This project derives direction and ideas from the Chancellor of Amrita University, Sri Mata Amritanandamayi Devi. This work was supported by the Department of Science and Technology, CSI Grant No. SR/CSI/49/2010 and the Sakshat Project of National Mission on Education through ICT, Department of Higher Education, Ministry of Human Resource Department, Government of India.

References

Albus, J.S., 1971. A theory of cerebellar function. Math. Biosci. 10, 25–61.
Bao, S., Chen, L., Kim, J.J., Thompson, R.F., 2002. Cerebellar cortical inhibition and classical eyeblink conditioning. PNAS 99, 1592–1597.
Bedard, C., Kroger, H., Destexhe, A., 2004. Modeling extracellular field potentials and the frequency-filtering properties of extracellular space. Biophys. J. 86, 1829–1842.
Bower, J.M., Woolston, D.C., 1983. Congruence of spatial organization of tactile projections to granule cell and purkinje cell layers of cerebellar hemispheres of the albino rat: vertical organization of cerebellar cortex. J. Neurophysiol. 49, 745–766.
Brock, L.G., Coombs, J.S., Eccles, J.C., 1951. Action potentials of motoneurones with intracellular electrode. Proc. Univ. Otago Med. School 29, 14–15.
Chadderton, P., Margrie, T.W., Hausser, M., 2004. Integration of quanta in cerebellar granule cells during sensory processing. Nature 428, 856–860.
Chan-Palay, V., Palay, S.L., 1972. The form of velate astrocytes in the cerebellar cortex of monkey and rat: high voltage electron microscopy of rapid Goli preparations. Z. Anat. Entwickl.-Gesch. 138, 1–19.
D'Angelo, E., De Filippi, G., Rossi, P., Taglietti, V., 1995. Synaptic excitation of individual rat cerebellar granule cells in situ: evidence for the role of NMDA receptors. J. Physiol. (Lond.) 484, 397–413.
D'Angelo, E., De Filippi, G., Rossi, P., Taglietti, V., 1998. Ionic mechanism of electroresponsiveness in cerebellar granule cells implicates the action of a persistent sodium current. J. Neurophysiol. 80, 493–503.
D'Angelo, E., Nieus, T., Maffei, A., Armano, A., Rossi, P., Taglietti, V., Fontana, A., Naldi, G., 2001. Theta-frequency bursting and resonance in cerebellar granule cells: experimental evidence and modeling of a slow K^+ dependent mechanism. J. Neurosci. 21, 759–770.
D'Errico, A., Prestori, F., D'Angelo, E., 2010. Extending the bandwidth of long-term plasticity at the cerebellar input stage. J. Physiol. 588, 5–6.
Diwakar, S., Magistretti, J., Goldfarb, M., Naldi, G., D'Angelo, E., 2009. Axonal Na^+ channels ensure fast spike activation and back-propagation in cerebellar granule cells. J. Neurophysiol. 101, 519–532.
Diwakar, S., Lombardo, P., Solinas, S., Naldi, G., D'Angelo, E., 2011. Local field potential modeling predicts dense activation in cerebellar granule cells clusters under LTP and LTD control. PLoS ONE 6 (7), e21928. doi:10.1371/journal.pone.0021928.
Eccles, J.C., Ito, M., Szentagothai, J., 1967. The Cerebellum as a Neuronal Machine. Springer, Berlin.
Garwicz, M., Joerntell, H., Ekerot, C.F., 1998. Cutaneous receptive fields and topography of mossy fibres and climbing fibres projecting to cat cerebellar C3 zone. J. Physiol. (Lond.) 512, 277–293.
Gold, C., Henze, D.A., Koch, C., Buzsaki, G., 2006. On the origin of the extracellular action potential waveform: a modeling study. J. Neurophysiol. 95, 3113–3128.
Gold, C., Henze, D.A., Koch, C., 2007. Using extracellular action potential recordings to constrain compartmental models. J. Comput. Neurosci. 23, 39–58.
Haberly, L., Shepherd, G.M., 1973. Current density analysis of summed evoked potentials in opossum prepyriform cortex. J. Neurophysiol. 36, 789–803.
Henze, D.A., Borhegyi, Z., Csicsvari, J., Mamiya, A., Harris, K., Buzsaki, G., 2000. Intracellular features predicted by extracellular recordings in the hippocampus in vivo. J. Neurophys. 83, 390–400.
Hines, M.L., Carnevale, N.T., 1997. The NEURON simulation environment. Neural Comput. 9, 1179–1209.
Hines, M.L., Carnevale, N.T., 2001. NEURON: a tool for neuroscientists. The Neuroscientist 7, 123–135.
Holt, G.R., Koch, C., 1999. Electrical interactions via the extracellular potential near cell bodies. J. Comput. Neurosci. 6, 169–184.
Jorntell, H., Eckerot, C.F., 2006. Properties of somatosensory synaptic integration in cerebellar granule cells in vivo. J. Neurosci. 26, 11786–11797.
Katz, D.B., Steinmetz, J.E., 1997. Single-unit evidence for eye-blink conditioning in cerebellar cortex is altered. Learning and Memory (Cold Spring Harbor Laboratory Pres 3).
Logothetis, N.K., 2002. The neural basis of the blood-oxygen-level dependent functional magnetic resonance imaging signal. Philos. Trans. Roy. Soc. Lond. B Biol. Sci. 357, 1003–1037.
Mapelli, J., D'Angelo, E., 2007. The spatial organization of long-term synaptic plasticity at the input stage of cerebellum. J. Neurosci. 27, 1285–1296.
Marr, D.A., 1969. A theory of cerebellar cortex. J. Physiol. (Lond.) 202, 437–470.
Mitzdorf, U., 1985. Current source–density method and application in cat cerebral cortex: investigation of evoked potentials and EEG phenomena. Physiol. Rev. 65, 37–100.
Nieus, T., Sola, E., Mapelli, J., Saftenku, E., Rossi, P., D'Angelo, E., 2006. LTP regulates burst initiation and frequency at mossy fiber – granule cell synapses of rat cerebellum: experimental observations and theoretical predictions. J. Neurophysiol. 95, 686–699.
Parasuram, H., Abdulmanaph, N., Nair, B., Diwakar, S., 2010. Modeling granular layer local field potential using single neuron and network based approaches to predict LTP/LTD in extracellular recordings. In: Proceedings of Neurocomp (Lyon, France), October 6–8, 2010.
Plonsey, R., 1969. Bioelectric Phenomena. McGraw-Hill Book Company, New York.
Rall, W., Shepherd, G.M., 1968. Theoretical reconstruction of field potentials and dendrodendritic synaptic interactions in the olfactory bulb. J. Neurophysiol. 31, 884–915.
Rancz, E.A., Ishikawa, T., Duguid, I., Chadderton, P., Mahon, S., 2007. High-fidelity transmission of sensory information by single cerebellar mossy fibre boutons. Nature 450, 1245–1248.
Roggeri, L., Rivieccio, B., Rossi, P., D'Angelo, E., 2008. Tactile stimulation evokes long-term synaptic plasticity in the granular layer of cerebellum. J. Neurosci. 28, 6354–6359.
Silver, R.A., Cull-Candy, S.G., Takahashi, T., 1996. Non-NMDA glutamate receptor occupancy and open probability at a rat cerebellar synapse with single and multiple release sites. J. Physiol. 494, 231–250.
Sola, E., Prestori, F., Rossi, P., Taglietti, V., D'Angelo, E., 2004. Increased neurotransmitter release during long-term potentiation at mossy fibre-granule cell synapses in rat cerebellum. J. Physiol. 557, 843–861.
Solinas, S., Nieus, T., D'Angelo, E., 2010. A realistic large-scale model of the cerebellum granular layer predicts circuit spatio-temporal filtering properties. Front. Cell. Neurosci. 4.
Uusisaari, M., De Schutter, E., 2011. The mysterious microcircuitry of the cerebellar nuclei. J. Physiol. doi:10.1113/jphysiol.2010.201582.
Vos, B.P., Volny-Luraghi, A., De Schutter, E., 1999. Cerebellar Golgi cells in the rat: receptive fields and timing of responses to facial stimulation. Eur. J. Neurosci. 11, 2621–2634.